AIAA 81-0276R

Finite Element Analysis of Inviscid Subsonic Boattail Flow

R. V. Chima*
NASA Lewis Research Center, Cleveland, Ohio
and
P. M. Gerhart†
University of Akron, Akron, Ohio

A finite element code for analysis of inviscid subsonic flows over arbitrary nonlifting planar or axisymmetric bodies is described. The code solves a novel primitive variable formulation of the coupled irrotationality and compressible continuity equations. Results for flows over a cylinder, a sphere, and an NACA 0012 airfoil verify the code. Computed subcritical flows over an axisymmetric boattailed afterbody compare well with finite-difference results and experimental data. Iterative coupling with an integral turbulent boundary-layer code shows strong viscous effects on the inviscid flow. Improvements in code efficiency and extensions to transonic flows are discussed.

Introduction

MODERN tactical aircraft usually have one or two jet engines within the fuselage, with the jet exhausts exiting through axisymmetric nozzles at the rear. Integration of the afterbody and nozzle, or boattail region (Fig. 1), with the fuselage can effect aircraft performance strongly.[1] Indeed, the boattail drag can be as much as 20% of the total aircraft drag at transonic speeds.

Several flow phenomena contribute to the boattail drag. The boattail is immersed in the thick turbulent boundary layer that develops over the fuselage. The flow undergoes a drag producing expansion onto the boattail followed by a recompression onto the jet wake, with possible shocks and separation adding to the drag. Finally, the high velocity jet displaces and entrains the external flow, thereby modifying the boattail pressure distribution. If the jet entrainment is neglected, the jet may be modeled as a solid body or sting.

This paper describes a new finite element (FE) method for solving the primitive variable equations of inviscid subsonic flow about arbitrary axisymmetric or two-dimensional symmetric bodies. Subcritical flow over a boattail model, including viscous interaction using an integral boundary-layer method, served as the primary test of the method.

Many computational methods for the boattail problem have been published. Here they are grouped by the method used for the inviscid flow. An integral equation method for incompressible inviscid flows was coupled with an integral boundary-layer method in Ref. 2. The classical axisymmetric transonic full potential finite-difference (FD) boattail solution is given in Ref. 3. References 4 and 5 built on Ref. 3 by adding boundary-layer and exhaust plume effects. Similar but independent methods were used in Refs. 6 and 7. Reference 8 is an extension of Ref. 6 to three dimensions and angle of attack. The axisymmetric Navier-Stokes equations were solved by FD methods in Refs. 9 and 10 and by a FE method in Ref. 11. A three-dimensional Navier-Stokes FD solution for supersonic flows over ogive cylinder-boattails was presented in Ref. 12. Additionally, an experimental study of boattail drag is given in Ref. 13. To our knowledge, Ref. 11 is the only other FE solution of the boattail problem.

Many applications of FE methods to other inviscid flow problems have been published recently. Incompressible potential flows were considered in Refs. 14 and 15. Subcritical potential flows were solved in two dimensions in Refs. 16 and 17 and in three dimensions in Ref. 18. References 19-22 solved two-dimensional transonic potential flows and Ref. 23 included three-dimensional transonic flows. Primitive variable FE methods are described in Ref. 24 for subcritical flows and in Ref. 25 for transonic flows. The method described in Ref. 25 is somewhat similar to the one described here.

In the present work a FE method was used to solve a novel formulation of inviscid flow. The equations solved here, referred to as the nonhomogeneous Cauchy-Riemann equations in Ref. 26, consist of a compressible continuity equation and the irrotationality condition. Both are first-order equations for the velocity components. Steady first-order equations are difficult to solve by FD techniques but simplify the FE formulation by allowing first-order interpolation functions. The form of the compressible continuity equation used reduces to the incompressible equation as $M_\infty \to 0$. Compressible flows are solved iteratively, starting with the incompressible solution. The iterative scheme converges rapidly for subsonic flows.

Flows over simple geometries have been computed and are presented to verify the method. Boattail solutions are com-

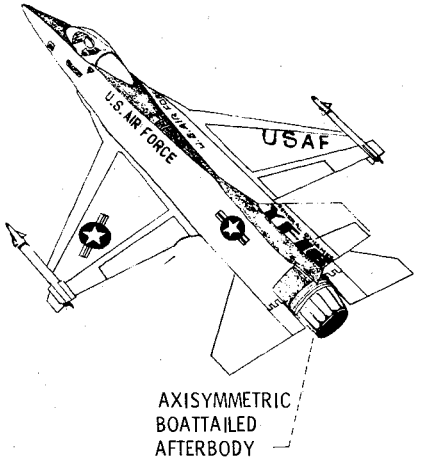

Fig. 1 Boattail afterbody on an F-16 aircraft. The F-16 has very low afterbody drag.[1]

Presented as Paper 81-0276 at the AIAA 19th Aerospace Sciences Meeting, St. Louis, Mo., Jan. 12-15, 1981; submitted Feb. 23, 1981; revision received July 1, 1981. This paper is declared a work of the U.S. Government and therefore is in the public domain.

*Research Engineer, Computational Fluid Mechanics Branch. Member AIAA.

†Associate Professor, Mechanical Engineering Department.

pared to a surface source solution for incompressible flow and to a FD solution[6] for compressible flow. An integral boundary-layer method[27] was coupled iteratively with the inviscid calculation. Viscous boattail results are compared to experimental data from Ref. 13. Finally, methods for improving the computational efficiency of the scheme and for extending it to transonic flows are discussed.

Equations and Boundary Conditions

As derived in Ref. 28, the axisymmetric inviscid continuity equation for isentropic flow is

$$\frac{\partial u}{\partial x}+\frac{\partial v}{\partial y}+j\frac{v}{y}-M_\infty^2\left\{\left[\frac{(1-\gamma)}{2}+\frac{(\gamma+1)}{2}u^2+\frac{(\gamma-1)}{2}v^2\right]\frac{\partial u}{\partial x}\right.$$
$$+\left[\frac{(1-\gamma)}{2}+\frac{(\gamma-1)}{2}u^2+\frac{(\gamma+1)}{2}v^2\right]\frac{\partial v}{\partial y}$$
$$\left.+\frac{(\gamma-1)}{2}(u^2+v^2-1)j\frac{v}{y}+2uv\frac{\partial u}{\partial y}\right\}=0 \qquad (1)$$

where all velocities are normalized by the freestream velocity and all lengths by an arbitrary length scale. The axisymmetric terms are multiplied by a switching integer j, such that $j=1$ gives the axisymmetric equation and $j=0$ gives the two-dimensional equation.

This equation is solved simultaneously with the normalized irrotationality condition

$$\frac{\partial u}{\partial y}-\frac{\partial v}{\partial x}=0 \qquad (2)$$

The normalized boundary conditions are the freestream conditions

$$\text{as } x,y\to\pm\infty,\quad u\to 1,\quad v\to 0 \qquad (3)$$

and the tangency condition at a solid surface

$$V_{nb}=v_b\cos\theta_b-u_b\sin\theta_b=0 \qquad (4)$$

where u_b and v_b are the x and y velocity components on a surface at angle θ_b to the x axis. Equations (1) and (2) are equivalent to the nonconservative full potential equation. Note that Eq. (2) is linear and Eq. (1) is of the form: linear continuity equation $-M_\infty^2$* nonlinear terms $=0$ so that as $M_\infty\to 0$ the equation set becomes linear.

Finite Element Formulation

The dependent variables u and v, and for axisymmetric flow the independent variable y, are approximated within arbitrary quadrilateral FE's by interpolations of the form

$$u=\Omega_N u_N \quad v=\Omega_N v_N \quad y=\Omega_N y_N \quad N=1,2,3,4 \qquad (5)$$

where Ω_N are bilinear interpolation functions dependent on element geometry, u_N, v_N, and y_N are values of u, v, and y at node N, and the summation convention is implied.

Substitution of the approximations of Eq. (5) into the equations of motion Eqs. (1) and (2) results in residual errors which are minimized by the Galerkin method, a subclass of the method of weighted residuals. The Galerkin formulation of Eq. (2) results in

$$\int_A \Omega_N\frac{\partial\Omega_M}{\partial y}y^j\,dy\,dx\,u_M-\int_A\Omega_N\frac{\partial\Omega_M}{\partial x}y^j\,dy\,dx\,v_M=0 \qquad (6a)$$

which may be written as

$$A_{NM}u_M+B_{NM}v_M=0 \qquad N,M=1,2,3,4 \qquad (6b)$$

Similar application of the Galerkin method to Eq. (1) gives the system of equations

$$\left[\begin{array}{c|c} C-M_\infty^2[F(u^{n-1},v^{n-1}) & (D+jE)-M_\infty^2[H(u^{n-1},v^{n-1}) \\ \quad +G(u^{n-1},v^{n-1})] & \quad +jI(u^{n-1},v^{n-1})] \\ \hline A & B \end{array}\right] \times\left[\begin{array}{c} u^n \\ \hline v^n \end{array}\right]=0 \qquad (7)$$

where subscripts N and M have been omitted for clarity.

Equation (7) represents eight algebraic equations in eight unknowns—the eight velocity components $[u_M,v_M]^T$ at the four nodes M of an element. Terms A through I are 4×4 coefficient matrices given in Appendix A and are evaluated numerically by two point Gaussian quadrature. Superscripts n refer to iteration number. Equation (7) may be written for each element of a flowfield, then assembled into a global matrix equation. It can be shown that the assembled equations are second-order accurate.

Numerical Treatment of Boundary Conditions

Inflow and freestream conditions on u and v in Eq. (3) are applied at a finite distance from the body by direct substitution into the global matrix equation. Elimination of these terms would have been computationally more efficient but was not done. Along symmetry axes and the outflow boundary the v velocity component was set to zero and the u component was solved for from the flow equations. Resulting values of u along the outlet were within a fraction of a percent of the freestream values. However, when the u components at the outlet were fixed at exactly their freestream values, the global matrix equation became singular.

Flow tangency conditions Eq. (4) were applied using a Lagrange multiplier technique discussed in Ref. 29 and in Appendix B. This technique introduces an auxiliary constraint equation with a nonphysical unknown at each body node. Because of the extra unknowns, the technique is inefficient and would not be recommended for future work.

Iterative Solution Method

Terms $F(u,v)$ through $I(u,v)$ in Eq. (7) are nonlinear functions of the nodal unknowns and are evaluated iteratively. For the first iteration ($n=1$) the terms F through I are set to zero and the resulting set is solved using a Gauss elimination scheme for banded matrices, giving the incompressible solution. In subsequent iterations the nonlinear terms are evaluated from the previous values of u and v. This scheme is equivalent to lagging the density calculation, and is unconditionally stable for subsonic flows. Convergence is extremely rapid, with all $u^{n+1}-u^n$ and $v^{n+1}-v^n$ less than 10^{-4} in 5-7 iterations.

Viscous-Inviscid Interaction

The FE inviscid flow code was coupled iteratively with a Sasman-Cresci[27] type integral boundary-layer code by the classical method of augmentation of the body by the displacement thickness. Compressible inviscid calculations were allowed to fully converge before the viscous corrections were made. It was shown in Ref. 6 that considerable computational time can be saved by using partially converged inviscid solutions to update the boundary layer, but this was not attempted.

Computational Grid

Sheared grids, as illustrated at the tops of Figs. 4 and 6, were used for each FE solution mentioned later. The band-

width of the global matrix that must be stored and solved is proportional to the number of nodes along a vertical grid line; so the vertical extent of the grid was kept small. Solution "wiggles" were often noted on highly elongated elements. They represent the highest frequency components of the continuum solution that can be resolved by the discrete solution, their wavelength being twice the grid spacing. The magnitude of the wiggles was typically in the fourth significant figure of the velocity components for incompressible solutions and did not increase appreciably for compressible flows. The nondissipative algorithm presented here cannot eliminate the high-frequency wiggles, but they can be reduced by other means. In this paper solution wiggles have been eliminated by plotting flow quantities evaluated at element midpoints using interpolation Eq. (5). This introduces exactly enough smearing to remove the highest frequency wiggles. Since wiggles are related to element spacing, they could presumably be lessened by using less distorted grids such as the wrap around grids described in Ref. 30. It may also be possible to reduce wiggles by using downstream boundary conditions that are less restrictive than Eq. (3), such as simple extrapolation of the velocity components.

Verification Results

Figures 2 and 3 show calculated pressure coefficients on a sphere and a cylinder, respectively. The symmetric solutions are shown only over the second quadrant, although both solutions were computed over the upper half plane. The same coarse 9×53 node grid (17 points on the body) was used for both calculations. Incompressible FE solutions agree well with the analytic solutions. Compressible results at $M_\infty=0.5$ for the sphere and $M_\infty=0.38$ for the cylinder, both near their critical Mach numbers, agree reasonably well with those predicted by a Gothert rule compressibility transformation of the analytic incompressible solution.

Flow over a nonlifting NACA 0012 airfoil at $M_\infty=0.7$ was computed on the 18×47 node grid shown at the top of Fig. 4. Nineteen points were distributed over the body at the locations tabulated in Abbot and Von Doenhoff.[31] The lower half of Fig. 4 shows the computed Mach number contours at $M_\infty=0.7$. Computed incompressible and compressible pressure coefficients are compared with experimental data from Refs. 31 and 32, respectively, in Fig. 5, with good agreement in both cases.

Boattail Results

Computed pressure distributions for a boattail model are compared with experimental data from Ref. 13, which also gives details of the geometry. Briefly, the boattail model, which is sketched in Fig. 7, starts with a 10-deg half-angle conical nose followed by a long cylindrical centerbody. The boattail region, which makes up about 9% of the model

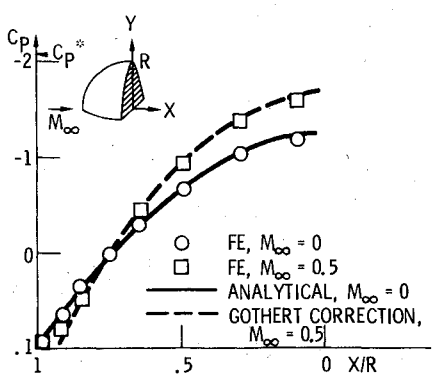

Fig. 2 Computed and analytical pressure coefficients on a sphere, $M_\infty=0, 0.5$.

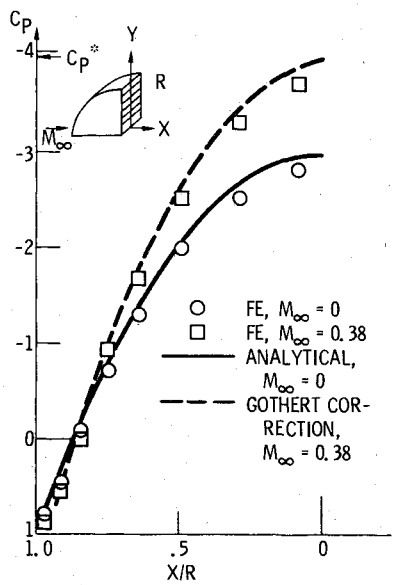

Fig. 3 Computed and analytical pressure coefficients on a cylinder, $M_\infty=0, 0.38$.

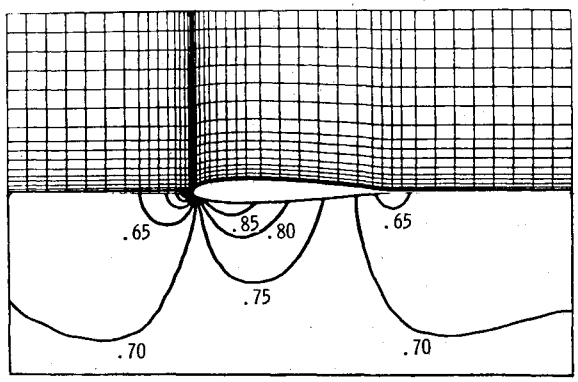

Fig. 4 Top: NACA 0012 airfoil grid; bottom: Mach number contours, $M_\infty=0.7$, contour increment = 0.05.

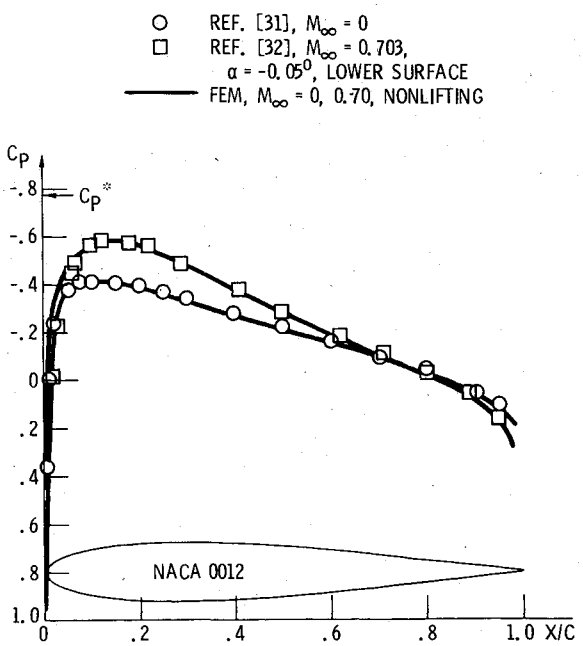

Fig. 5 Computed and measured pressure distributions for a nonlifting NACA 0012 airfoil, $M_\infty=0, 0.7$.

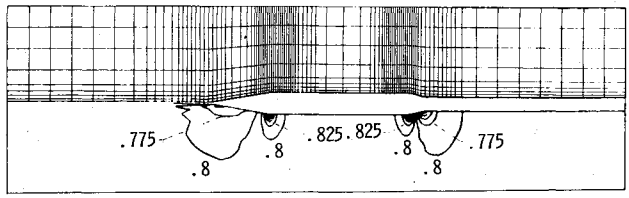

Fig. 6 Top: Boattail grid; bottom: Mach number contours, $M_\infty = 0.8$, contour increment = 0.025.

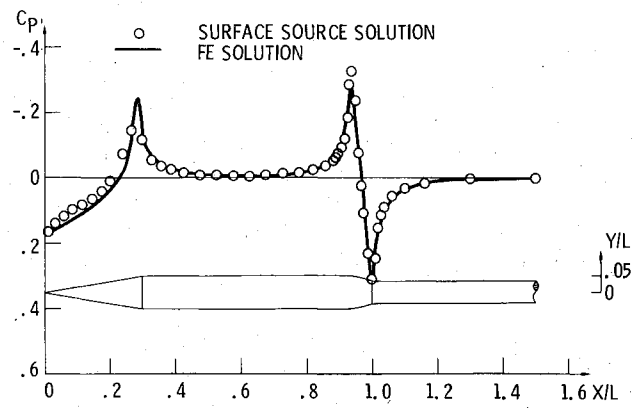

Fig. 7 Comparison of FE and surface source solutions for the incompressible pressure distribution over a boattail model.

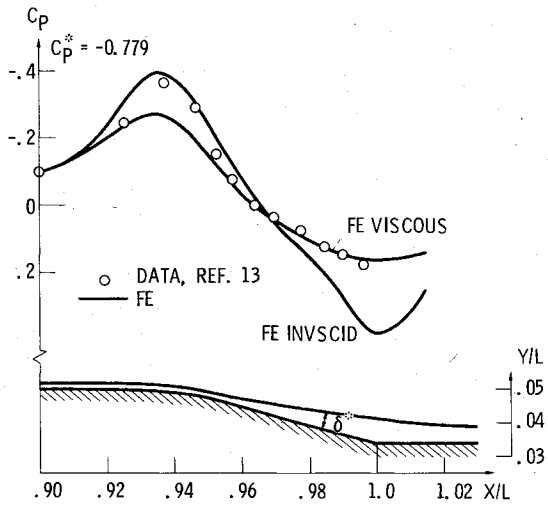

Fig. 8 Boattail pressure distributions, $M_\infty = 0.7$, $Re_L = 1.3413 \times 10^7$; comparison of FE calculations and data.

(excluding the sting) consists of a spherical section that smoothly joins the centerbody to a 15-deg conically necked-down section. The model is mounted on a long cylindrical sting representing a propulsive jet.

Figure 6 shows a 10×102 node grid (85 points on the body, 9 over the boattail region) used for the boattail computations. The lower half of the figure shows computed Mach number contours at $M_\infty = 0.8$.

Incompressible results for the boattail are compared with a surface source solution in Fig. 7. Agreement is good over the entire body except near the nose, where the source distribution in the surface source solution was probably inadequate. A good incompressible FE solution is important since it acts as a starting point of the compressible iteration.

A subcritical solution over the boattail region, both with and without viscous interaction, is compared with experimental data in Fig. 8. The freestream Mach number is $M_\infty = 0.7$ and the Reynolds number based on body length

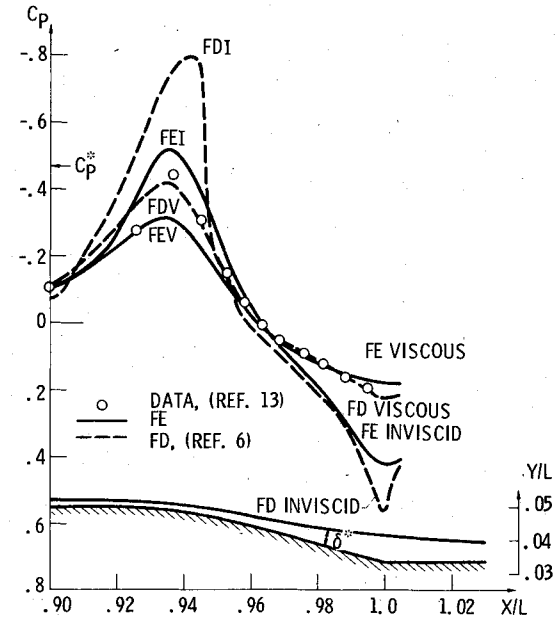

Fig. 9 Boattail pressure distributions, $M_\infty = 0.8$, $Re = 1.4181 \times 10^7$; comparison of FE and FD calculations and experimental data.

excluding sting is $Re_L = 1.3413 \times 10^7$. The viscous solution underpredicts the initial expansion but agrees well with the data in the recompression over the boattail and onto the sting. The figure illustrates the strong effect that a thick boundary layer can have on an inviscid pressure distribution. At the bottom of the figure the actual body is shown with the equivalent displacement body, illustrating the smoothing effect the boundary layer has on the boattail-sting juncture.

A small trick was needed to compute the viscous flows shown in Figs. 8 and 9. In the first iteration of the inviscid-viscous interaction, the boundary-layer code invariably predicted separation in response to the strong inviscid pressure gradient near the end of the boattail. However, the converged interaction shows no separation. To avoid separation at the first iteration, the inviscid solution was first converged at $M_\infty = 0.2$. The boundary layer did not separate in response to this pressure field, so an equivalent displacement body could be determined. Subsequent inviscid solutions at the desired Mach number but over the current displacement body were enough smoothed that the boundary layers did not separate, and the inviscid-viscous interaction could be converged.

Another boattail solution at $M_\infty = 0.8$ and $Re_L = 1.418 \times 10^7$ is shown in Fig. 9. (Mach number contours for the inviscid solution are shown in Fig. 6.) The inviscid solution is interesting in that it shows supersonic velocities at four nodes. The FE formulation is purely elliptic and contains no upwind bias in supercritical regions. Without special treatment FD relaxation schemes typically diverge for supercritical flows. In fact, the FE solution also diverges at slightly higher M_∞. It is thought that the direct solution of the FE equations over the entire flowfield is responsible for the method's ability to converge with slightly supercritical flow.

Also shown in Fig. 9 is the FD nonconservative transonic potential solution for the same problem by Chow et al. The FD solution, which includes upwind differencing in supersonic regions, predicts a strong shock recompression on the boattail. This shock is eliminated completely when the viscous interaction is considered. The FE and FD codes use the same boundary layer code, but the FD solution shows better agreement with the viscous data. This may be due to differences in treatment of the freestream boundary, which is mapped to infinity in the FD code but is placed about 10 body radii away in the FE code.

Computer Requirements

Both the FE and FD codes were run on an IBM 370/158 computer. CPU times for inviscid solutions such as those shown in Fig. 9 were 760 s for the FE solution and 260 s for the FD solution on similar grids. The FE code has since been cleaned up and run on an IBM 3033. The inviscid solution in Fig. 9 took about 34 s and the interaction solution took about 170 s. The FE solution required over one million words of storage, about 13 times that required by the FD code, principally for storage of the global coefficient matrices. Storage requirements are not much of a problem on a virtual storage computer, as page faults can be minimized by accessing the global matrix only columnwise.

Discussion and Conclusions

A FE solution of the first-order equations of inviscid, irrotational compressible flow has been developed, verified, and applied to the analysis of subsonic flow over a boattail. Reasonable agreement with experimental boattail data was obtained when the inviscid code was coupled with an integral boundary-layer code. Two-dimensional inviscid-viscous interaction calculations were made quickly, and thus appear to be useful tools for screening boattail afterbody designs prior to more extensive calculations or wind tunnel testing.

Certain aspects of this FE algorithm are appealing. First, FE methods are able to fit arbitrary boundaries, with the mapping to computational space contained in the element formulation rather than in transformation of the flow equations. Incidentally, the interpolation functions for the flow variables also are useful when flow variables are needed at off-node points, for example, when calculating a detailed pressure distribution for boundary layer coupling. Second, the primitive variable formulation allows use of bilinear interpolation functions, guarantees a continuous velocity and density solution, and eliminates the need to differentiate a potential function. However, solving two equations per node lengthens solution time. Finally, the ability of the method to model the first-order primitive variable equations even at sonic velocities and without convergence problems suggests that direct solvers may be useful for other two-dimensional problems.

The FE code was slower than an existing FD code, but CPU times for the FE code could be reduced by code refinement. Time spent in Gaussian solution of the global matrix equations could be reduced by vectorization for a vector computer.

The artificial compressibility technique developed by Hafez[19] could be used to extend the present method to transonic flows. Here the continuity equation would be written in conservative form. The density calculation is lagged, and upwinded at supersonic nodes. Since the conservative form of the continuity equation has many fewer terms than Eq. (1), the artificial compressibility technique should also improve the computational efficiency of the method.

Appendix A

Terms A_{NM} through I_{NM} in Eq. (7) are 4×4 coefficient matrices resulting from the Galerkin FE formulation of the irrotationality and continuity equations, and are given by

$$A_{NM}=\int_A \Omega_N \frac{\partial\Omega_M}{\partial y} y^j \mathrm{d}y\mathrm{d}x, \quad B_{NM}=-\int_A \Omega_N \frac{\partial\Omega_M}{\partial x} y^j \mathrm{d}y\mathrm{d}x$$

$$C_{NM}=-B_{NM}, \quad D_{NM}=A_{NM}, \quad E_{NM}=\int_A \Omega_M\Omega_N \mathrm{d}y\mathrm{d}x$$

$$F_{NM}=\int_A \left[\frac{(1-\gamma)}{2}+\frac{(\gamma+1)}{2}(\Omega_L u_L)^2 + \frac{(\gamma-1)}{2}(\Omega_L v_L)^2\right]\Omega_N \frac{\partial\Omega_M}{\partial x} y^j \mathrm{d}y\mathrm{d}x$$

$$G_{NM}=2\int_A (\Omega_K u_K)(\Omega_L v_L)\frac{\partial\Omega_M}{\partial y}\Omega_N Y^j \mathrm{d}y\mathrm{d}x$$

$$H_{NM}=\int_A \left[\frac{(1-\gamma)}{2}+\frac{(\gamma-1)}{2}(\Omega_L u_L)^2 + \frac{(\gamma+1)}{2}(\Omega_L v_L)^2\right]\Omega_N \frac{\partial\Omega_M}{\partial y} y^j \mathrm{d}y\mathrm{d}x$$

$$I_{NM}=\frac{(\gamma-1)}{2}\int_A \left[(\Omega_L u_L)^2+(\Omega_L v_L)^2-1\right]\Omega_N\Omega_M \mathrm{d}y\mathrm{d}x$$

$$K,L,M,N=1,2,3,4$$

Terms A_{NM} through E_{NM} are functions of known interpolation functions Ω_N. Terms F_{NM} through I_{NM} also include the nodal unknowns u_L and v_L and must be evaluated iteratively. All integrals were evaluated numerically in the present work; however, computer time could probably be saved by evaluating some of the integrals analytically.

Appendix B—Lagrange Multiplier Technique for Tangency Conditions

The tangency condition Eq. (4) can be written as

$$u\tan\theta - v = 0$$

with subscripts b deleted to avoid confusion. To impose tangency conditions at m nodes they are written as

$$f_{ri}u_i + g_{ri}v_i = 0 \qquad r=1,2,\ldots,m \tag{B1}$$

where

$f_{ri}=\tan\theta_i$ if the rth tangency condition applies to node i

$=0$ otherwise

$g_{ri}=-1$ if the rth tangency condition applies to node i

$=0$ otherwise

Following Ref. 29, boundary conditions Eqs. (B1) are incorporated in the system of Eq. (7) (the incompressible form is shown subsequently for simplicity) by introduction of a Lagrange multiplier λ_r as follows:

$$\left[\begin{array}{c|c|c} C_{NM} & D_{NM}+jE_{NM} & f_{rN} \\ \hline A_{NM} & B_{NM} & g_{rN} \\ \hline f_{rM} & g_{rM} & 0 \end{array}\right] \left[\begin{array}{c} u_M \\ \hline v_M \\ \hline \lambda_r \end{array}\right] = 0 \quad \begin{array}{l} N,M=1,2,3,4 \\ r=1,2,\ldots,m \end{array} \tag{B2}$$

Equation (B2) may be solved for the nodal velocities u_M and v_M now subject to the tangency conditions Eqs. (B1) at m nodes. Equation (B2) must also be solved for m Lagrange multipliers λ_r which are not used.

Boattail results shown in Figs. 7-9 had 85 points on the body requiring the solution of 85 additional constraint equations, with an accompanying increase in computer storage and time. A more efficient (but more difficult to program) method for imposing tangency conditions would be to use Eq. (4) to algebraically eliminate one unknown velocity at each surface node from the system of Eq. (7).

Acknowledgments

Much of this work was supported by the U.S. Army Research Office under Grants DAHCO4-75-G-0026 and DAAG-77-0030.

References

[1] Hunt, B. L., Surber, L. E., and Grant, G. K., "Propulsion-System Integration for Tactical Aircraft," *Astronautics & Aeronautics*, Vol. 18, June 1980, pp. 62-68.

[2] Nakayama, A., Patel, V. C., and Landweber, L., "Flow Interaction Near the Tail of a Body of Revolution, I—Flow Exterior to Boundary Layer and Wake, II—Iterative Solution for Flow Within and Exterior to Boundary Layer and Wake," *Journal of Fluids Engineering*, Vol. 98, Sept. 1976, pp. 531-546.

[3] South, J. C. Jr. and Jameson, A., "Relaxation Solutions for Inviscid Axisymmetric Transonic Flow Over Blunt or Pointed Bodies," *AIAA Computational Fluid Dynamics Proceedings*, Palm Springs, Calif., July 1973, pp. 8-17.

[4] Cosner, R. R. and Bower, W. W., "A Patched Solution of the Transonic Flowfields About an Axisymmetric Boattail," AIAA Paper 77-227, Jan. 1977.

[5] Kuhn, G. D., "Computer Program for Calculation of Separated Turbulent Flows on Axisymmetric Afterbodies," Arnold Engineering Development Center Rept. AEDC-TR-77-72, June 1977.

[6] Chow, W. L., Bober, L. J., and Anderson, B. H., "Numerical Calculation of Transonic Boattail Flow," NASA TN D-7984, June 1975.

[7] Wilmoth, R. G., "Computation of Transonic Boattail Flow with Separation," NASA TP-1070, Dec. 1977.

[8] Nakayama, A. and Chow, W. L., "Calculations of Transonic Boattail Flow at Small Angle of Attack," Univ. of Illinois, Champaign-Urbana, Ill., Rept. ME-TN-395-6, April 1979 (NASA CR-158471).

[9] Holst, T. L., "Numerical Solution of Axisymmetric Boattail Flow Fields with Plume Simulators," AIAA Paper 77-224, Jan. 1977.

[10] Cosner, R. R., "Fast Navier-Stokes Solution of Transonic Flowfields About Axisymmetric Afterbodies," AIAA Paper 80-0193, Jan. 1980.

[11] Cooke, C. H. and Blanchard, D. K., "A Shock Capturing Application of the Finite Element Method," *International Journal for Numerical Methods in Engineering*, Vol. 14, Feb. 1979, pp. 271-286.

[12] Schiff, L. B. and Sturek, W. B., "Numerical Simulation of Steady Supersonic Flow Over an Ogive-Cylinder-Boattail Body," AIAA Paper 80-0066, Jan. 1980.

[13] Shrewsbury, G. D., "Effect of Boattail Juncture Shape on Pressure Drag Coefficient of Isolated Afterbodies," NASA TM X-1517, March 1968.

[14] Baskharone, E. and Hamed, A., "A New Approach to Cascade Flow Analysis Using the Finite Element Method," AIAA Paper 80-0389, Jan. 1980.

[15] Keck, H. and Haas, W., "Vorticity and Blade Circulation Modelling in the Calculation of Quasi-Three-Dimensional Cascade Flows with Finite Elements," Third International Conference on Finite Elements in Flow Problems, Banff, Alberta, Canada, June 1980.

[16] Chima, R. V., "Finite Element Analysis of Inviscid Subsonic Flow with Viscous Interaction and Inverse Applications," Ph.D. Dissertation, Univ. of Akron, 1979; available from University Microfilms.

[17] Habashi, W. G., "Finite Element Approach to Compressor Blade-to-Blade Cascade Analysis," *AIAA Journal*, Vol. 27, July 1979, pp. 693-698.

[18] Laskaris, T. E., "Finite Element Analysis of Three-Dimensional Potential Flow in Turbomachines," *AIAA Journal*, Vol. 16, July 1978, pp. 717-722.

[19] Hafez, M. S. and Murman, E. M., "Artificial Compressibility Methods for Numerical Solution of Transonic Full Potential Equation," AIAA Paper 78-1148, July 1978.

[20] Ecer, A. and Akay, H. U., "Investigation of Transonic Flow in a Cascade Using an Adaptive Mesh," AIAA Paper 80-1430, July 1980.

[21] Deconinck, H. and Hirsch, C. H., "A Finite Element Method Solving the Full Potential Equation with Boundary Layer Interaction in Transonic Cascade Flow," AIAA Paper 79-0132, Jan. 1979.

[22] Bristeau, M. O. et al., "Transonic Flow Simulations by Finite Elements and Least Square Methods," Third International Conference on Finite Elements in Flow Problems, Banff, Alberta, Canada, June 1980.

[23] Eberle, A., "Finite Element Methods for the Solution of Full Potential Equation in Transonic Steady and Unsteady Flow," Third International Conference on Finite Elements in Flow Problems, Banff, Alberta, Canada, June 1980.

[24] Fletcher, C.A.J., "A Primitive Variable Finite Element Formulation for Inviscid, Compressible Flow," *Journal of Computational Physics*, Vol. 33, Dec. 1979, pp. 301-312.

[25] Chattot, J. J., Guiu-Roux, J., and Laminie, J., "Finite Element Calculation of Steady Transonic Flow in Nozzles Using Primary Variables," 7th International Conference on Numerical Methods in Fluid Dynamics, Univ. of Stanford, Stanford, Calif., June 1980.

[26] Lomax, H. and Martin, E. D., "Fast Direct Numerical Solution of the Nonhomogeneous Cauchy-Reimann Equations," *Journal of Computational Physics*, Vol. 15, May 1974, pp. 55-80.

[27] Sasman, P. K. and Cresci, R. J., "Compressible Turbulent Boundary Layer with Pressure Gradient and Heat Transfer," *AIAA Journal*, Vol. 4, Jan. 1966, pp. 19-25.

[28] Liepmann, H. W. and Roshko, A., *Elements of Gas Dynamics*, Wiley, New York, 1957.

[29] Chung, T. J., *Finite Element Analysis in Fluid Dynamics*, McGraw-Hill, New York, 1978.

[30] Sorenson, R. L., "A Computer Program to Generate Two-Dimensional Grids About Airfoils and Other Shapes by the Use of Poisson's Equation," NASA TM-81198, May 1980.

[31] Abbott, I. H. and von Doenhoff, A. E., *Theory of Wing Sections*, Dover, New York, 1959.

[32] "Experimental Data Base for Computer Program Assessment," AGARD AR-138, May 1979.